J Mol Model (2012) 18:5133–5146
DOI 10.1007/s00894-012-1506-0

ORIGINAL PAPER

# Comparative study of the relaxation mechanisms of the excited states of cytosine and isocytosine

**Rumyana I. Bakalska · Vassil B. Delchev**

Received: 17 November 2011 / Accepted: 13 June 2012 / Published online: 10 July 2012


**Abstract** An experimental and theoretical investigation was performed to study the photostability of cytosine and isocytosine. The experimental UV irradiation of acetonitrile solutions of the two compounds showed that the amino-oxo tautomer of cytosine is photostable while the amino-oxo tautomer of isocytosine tautomerizes to the amino-hydroxy form. The theoretical investigations were carried out at the CC2 level of theory. They were performed to explain the experimental observations. It was found that the $^1\pi\pi^*$ excited states of the ring deformation mechanisms of cytosine and isocytosine relax (internal conversion) to the ground states of the amino-oxo forms of the compounds. We propose a channel for the radiationless deactivation of the repulsive $^1\pi\sigma^*$ excited state of the amino-oxo form of isocytosine to the ground state of the amino-hydroxy tautomer.

**Keywords** Coupled-cluster methods · Cytosine · Excited states · Isocytosine · Tautomerism · UV irradiation

## Introduction

Cytosine is one of the building blocks of the macromolecules of DNA and RNA. It is involved in the transmission and encoding of genetic information. Cytosine is a pyrimidine derivative which exhibits aromatic properties and considerable photostability.

Several papers [1, 2] have reported the UV absorption maxima of cytosine in the gas phase. The maximum at 4.6 (0.14) eV has been assigned to the $^1\pi \rightarrow \pi^*$ transition, while the maximum at 5.2 (0.03) eV was assigned to the $^1n_N \rightarrow \pi^*$ transition [1, 2]. Water solutions of cytosine show three absorption maxima at 4.65, 5.44 (shoulder), and 6.29 eV (the first is the least intensive), whereas four major bands are registered in acetonitrile at 4.54, 5.19, 5.79, and 6.20 eV (the last two bands are the most intensive ones) [3, 4]. Morita [3] has shown that the oxo N(1)H tautomer of cytosine is the most stable one in acetonitrile solution. Increasing the temperature of an acetonitrile solution of cytosine leads to the formation of the oxo N(3)H tautomer, but only in minor amounts [3]. Analysis of cytosine monohydrate in the crystal provides further evidence of the presence of oxo N(1)H tautomer [5].

A matrix isolation study of cytosine (evaporated at 493 K onto substrates at 15 K) showed the presence of two stable tautomers of cytosine: amino-oxo and amino-hydroxy [6]. The two tautomers of cytosine were identified by Nir [7] using jet-cooled and resonant multiphoton ionization experiments. The jet-cooled experiment performed by Brown gives an evidence for the presence of the imino-oxo tautomer of cytosine [8]. Logical explanations were provided by Tomić regarding the inability of some experiments to register the imino-oxo form of cytosine [9]: low transition moment of the imino tautomer, influence of the laser, etc. Kosma [10] reported that hydroxy or imino tautomers can be produced using UV sources (lasers, lamps) with wavelengths below 270 nm. On the other hand, some experiments have shown that the excited cytosine molecule relaxes back to the ground state via internal conversion on picosecond (1.86 ps) and femtosecond (160 fs) timescales, and no excited-state photoreactions are observed [10, 11]. These short lifetimes indicate that cytosine is highly stable. However, there is no clear and explicit explanation of the photostability of cytosine with respect to excited-state reaction mechanisms.

Crystal structure analysis of isocytosine has shown that it exists in the crystal state as two stable oxo tautomers: 1H- and 3H, in the ratio 1:1 [12, 13]. These tautomers are also seen in water solution [3].

Vranken et al. [14] have reported the IR spectrum of matrix-isolated isocytosine. It was demonstrated that the

R. I. Bakalska · V. B. Delchev (✉)
Faculty of Chemistry, University of Plovdiv,
Tzar Assen 24 Str.,
4000 Plovdiv, Bulgaria
e-mail: vdelchev@uni-plovdiv.bg

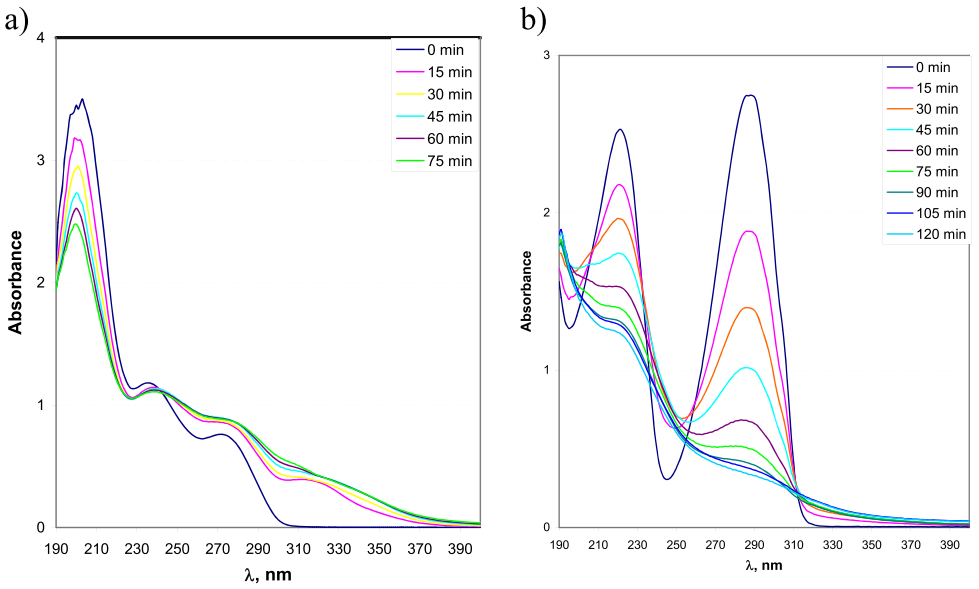


**Fig. 1a–b** UV spectra of irradiated (**a**) cytosine and (**b**) isocytosine in acetonitrile solution at different UV irradiation times

characteristic OH, $NH_2$, and NH stretching vibrations of the tautomers strongly overlap. However, one clear indication of the OH stretching vibration of hydroxy tautomer is the characteristic $\tau_{OH}$ band at ~520 $cm^{-1}$. The γ(C=O) vibration of the oxo(3H) tautomer gives a relatively informative band at 618 $cm^{-1}$ [14]. Vranken [14] also demonstrated that UV irradiation (λ=308 nm) of matrix-isolated isocytosine leads to the tautomerization of the amino-oxo tautomer to the amino-hydroxy form. This phototautomerization is accompanied by the photodecomposition of isocytosine. The by-product of this reaction shows very weak bands at 2342 and 2139 $cm^{-1}$ in an Ar matrix [14].

Several theoretical papers have reported excited-state geometries and possible pathways for the deactivation of excited states of nucleic acid bases [15–18]. Shukla et al. [15] have shown that the equilibrium geometry of the $^1\pi\pi^*$ excited state of isocytosine is highly nonplanar. However, the geometry of the second $^1n\pi^*$ excited state is planar [15]. Dynamics calculations have demonstrated that the deactivation of the $^1n\pi^*$ excited state of cytosine occurs with a time constant of 0.69 ps [17]. The deactivation is mediated by a semiplanar conical intersection [17].

The purpose of the current paper is to explain the high photostability of cytosine as compared to isocytosine upon UV irradiation. The research presented here comprises a study of the excited-state reaction paths of N–H dissociation and the ring deformation mechanisms of both compounds.

**Table 1** Kinetics of the photoreaction of isocytosine

| $t$ (min) | $\lambda_{max}$ (nm) | Abs | $k$ ($min^{-1}$) |
|---|---|---|---|
| 0 | 288 | 2.747584 | - |
| 15 | 286 | 1.883853 | 0.02516019 |
| 30 | 286 | 1.398445 | 0.02251204 |
| 45 | 285 | 1.016087 | 0.02210584 |
| 60 | 283 | 0.684288 | 0.02316831 |
| 75 | 280 | 0.518361 | 0.0222374 |
| $\bar{\lambda}_{max}$ = | **285** | | |
| | | $\bar{k}$ = | 0.02303676 |
| | | $\tau_{1/2}$ = | 30.08875 |

## Experimental methods

Cytosine and isocytosine were purchased from Fluka (Buchs, Switzerland) and Sigma, (St. Louis, MO, USA). Acetonitrile was obtained from Labscan (Super Gradient grade; Bangkok, Thailand).

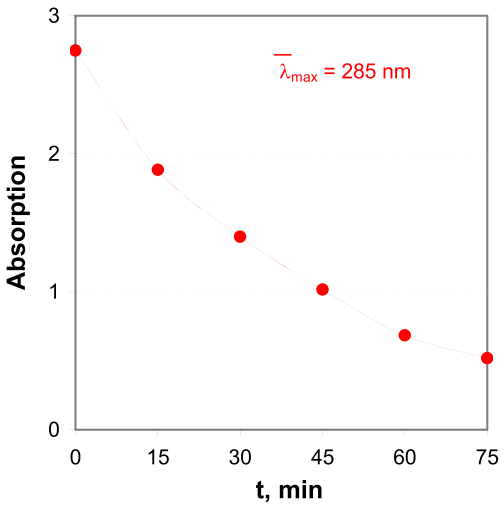


**Fig. 2** Evolution of the absorption over time for isocytosine

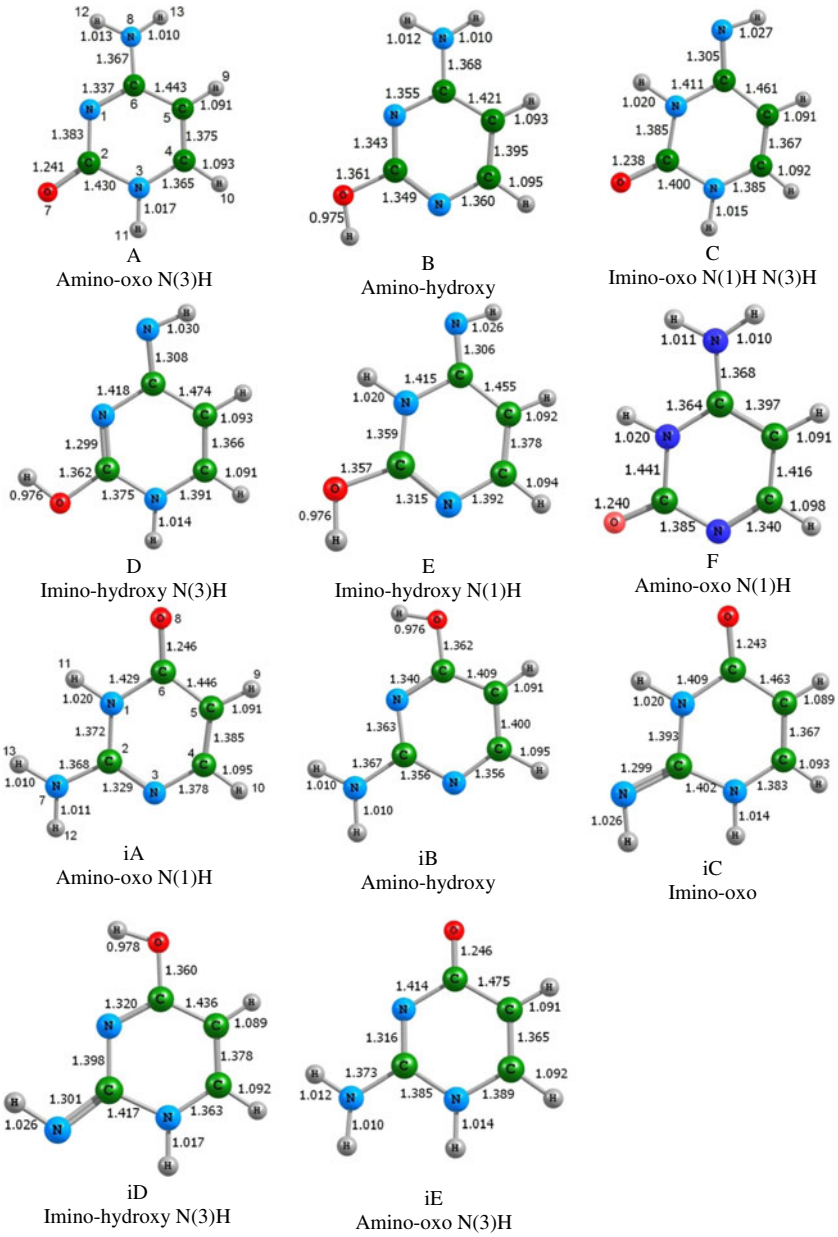


**Fig. 3** CC2-ground-state equilibrium geometries of the tautomers of cytosine and isocytosine

Photochemical irradiations were carried out in a standard Pyrex immersion reaction vessel. We used a high-pressure mercury lamp (TQ 150) with a quartz filter (Heraeus Noblelight, Hanau, Germany) as a UV light source.

We irradiated saturated solutions of cytosine and isocytosine in acetonitrile with UV light, $\lambda_{max}$=366 nm, for 75 min (cytosine solution) and 120 min (isocytosine solution). The results are shown in Fig. 1. Figure 1a indicates that cytosine is quite photostable under these conditions. The UV absorption maxima in Fig. 1b show that isocytosine is unstable and undergoes phototransformation for about 60 min. The UV absorption maximum of isocytosine at 285 nm was used to follow the photoreaction kinetics (see also Table 1).

The data in Table 1 explicitly show that the photoreaction of isocytosine is a first-order reaction (decomposition or isomerization) with a rate constant of 0.02304 $min^{-1}$ and a half-time $\tau_{1/2}$ = 30.089min. Figure 2, which illustrates the evolution of the absorbance over time, leads us to the same conclusion.

The course of the reaction was followed by performing UV spectroscopy every 15 min. The UV spectra (obtained using a 1 cm quartz cell) were taken with a PerkinElmer (Waltham, MA, USA) Lambda 9 UV-VIS/NIR spectrophotometer.

The IR spectra of the irradiated and unirradiated samples were recorded with a VERTEX 70 FT-IR spectrometer (Bruker Optics, Billerica, MA, USA) using KBr discs. After

**Table 2** CC2 vertical excitation energies of cytosine and isocytosine and the experimental UV-absorption maxima (in parentheses)

| A | | | B | | | C | | | D | | |
|---|---|---|---|---|---|---|---|---|---|---|---|
| State | eV | nm | State | eV | nm | State | eV | nm | State | eV | nm |
| $^1\pi\pi^*$ | 4.558 | 272 (271) | $^1\pi\pi^*$ | 4.878 | 254 | $^1\pi\pi^*$ | 5.005 | 248 | $^1\pi\pi^*$ | 4.686 | 265 |
| $^1n_O\pi^*$ | 4.800 | 259 | $^1n_N\pi^*$ | 5.118 | 242 | $^1\pi\sigma^*$ | 5.378 | 231 | $^1\pi\sigma^*$ | 4.930 | 252 |
| $^1n_N\pi^*$ | 5.260 | 236 | $^1\pi\sigma^*$ | 5.411 | 229 | $^1n_N\pi^*$ | 5.529 | 224 | $^1n_N\pi^*$ | 5.141 | 241 |
| $^1\pi\sigma^*$ | 5.322 | 233 | $^1\pi\pi^*$ | 5.806 | 214 | $^1\pi\pi^*$ | 5.769 | 215 | $^1\pi\sigma^*$ | 5.634 | 220 |
| $^1\pi\pi^*$ | 5.453 | 228 (236) | $^1n_N\pi^*$ | 5.814 | 213 | $^1\pi\sigma^*$ | 5.992 | 207 | $^1\pi\pi^*$ | 5.689 | 218 |
| $^1\pi\pi^*$ | 6.174 | 201 (203) | $^1\pi\pi^*$ | 6.317 | 196 | $^1\pi\pi^*$ | 6.218 | 199 | $^1\sigma\sigma^*$ | 5.833 | 212 |
| E | | | F | | | iA | | | iB | | |
| $^1\pi\pi^*$ | 4.377 | 284 | $^1\pi\pi^*$ | 4.174 | 297 | $^1\pi\pi^*$ | 4.574 | 271 (287) | $^1\pi\pi^*$ | 4.698 | 264 |
| $^1\pi\sigma^*$ | 5.188 | 239 | $^1n_N\pi^*$ | 4.579 | 271 | $^1n_O\pi^*$ | 4.881 | 254 | $^1n_N\pi^*$ | 5.098 | 243 |
| $^1n_N\pi^*$ | 5.542 | 224 | $^1\pi\sigma^*$ | 4.771 | 260 | $^1\pi\sigma^*$ | 5.079 | 244 | $^1\pi\sigma^*$ | 5.439 | 228 |
| $^1\pi\sigma^*$ | 5.762 | 215 | $^1n_O\pi^*$ | 5.002 | 248 | $^1n_N\pi^*$ | 5.734 | 216 | $^1\pi\pi^*$ | 5.796 | 214 |
| $^1\pi\pi^*$ | 5.795 | 214 | $^1\pi\sigma^*$ | 5.494 | 226 | $^1n_O\sigma^*$ | 5.846 | 212 (222) | $^1n_N\pi^*$ | 5.902 | 210 |
| $^1\pi\pi^*$ | 6.550 | 189 | $^1\pi\pi^*$ | 5.832 | 212 | | | | | | |
| iC | | | iD | | | iE | | | | | |
| $^1n_O\pi^*$ | 4.721 | 263 | $^1\pi\pi^*$ | 3.919 | 317 | $^1n_O\pi^*$ | 4.259 | 291 | | | |
| $^1\pi\pi^*$ | 4.844 | 256 | $^1\pi\sigma^*$ | 4.918 | 252 | $^1n_O\sigma^*$ | 4.752 | 261 | | | |
| $^1\pi\sigma^*$ | 5.055 | 245 | $^1n_N\pi^*$ | 5.458 | 227 | $^1n_O\pi^*$ | 4.955 | 250 | | | |
| $^1\pi\pi^*$ | 5.752 | 216 | $^1\pi\sigma^*$ | 5.584 | 222 | $^1\pi\sigma^*$ | 5.063 | 245 | | | |
| $^1\pi\sigma^*$ | 5.965 | 208 | $^1n_N\pi^*$ | 5.604 | 221 | $^1\pi\pi^*$ | 5.256 | 236 | | | |

irradiation the solvent of a small volume of solutions was removed by insufflation with nitrogen. The obtained solid residium was used for preparation of KBr discs.

## Computational methods

The ground-state equilibrium geometries of all planar tautomers of cytosine and isocytosine were optimized at the coupled-cluster CC2 level using aug-cc-pVDZ basis functions. We used the optimized geometries of the tautomers for subsequent frequency calculations performed at the MP2 level and with the same basis set.

The structures of the conical intersections discussed in this paper were optimized at the CASSCF(6,6)/6-31 G* level. The geometries of the nonplanar conical intersections and their GD (gradient difference) and DC (derivative coupling) vectors were used to generate 49 structures (points) on the narrow grid. The structures were produced by displacements along the GD and DC vectors, starting from the conical intersections. The generated structures were used to calculate the adiabatic surfaces ($W_1$ and $W_2$) in a limited space around the conical intersections.

The linear interpolation in internal coordinates (LIIC) approach was applied to interpolate between a given ground-state minimum geometry and a certain conical intersection, both of which were found at the CASSCF(6,6)/6-31 G* level. Each internal coordinate $Q_i$ of a given intermediate structure was found using the equation

$$Q_i = Q_i(\mathrm{c}) + \varepsilon.[Q_i(\mathrm{ci}) - Q_i(\mathrm{c})], \quad (1)$$

where $Q_i$(c) is the $i$th coordinate of the initial structure (tautomer), whereas $Q_i$(ci) is the same coordinate for the $S_0/S_1$ conical intersection; $\varepsilon$ is the interpolation parameter. The interpolation parameter is varied between 0 (at the ground-state minimum) and 1 (at the conical intersection). The adiabatic linearly interpolated reaction paths were calculated at the CC2/aug-cc-pVDZ level.

We performed relaxed scans of the repulsive $^1\pi\sigma^*$ excited states of the most stable tautomers of cytosine and isocytosine in order to study the N–H dissociation mechanisms. The N–H distance was used as a reaction coordinate. The remaining internal coordinates were left to relax. It is known that the dissociation of pyrimidines most commonly occurs through the repulsive $^1\pi\sigma^*$ excited state [19].

Second-order approximate coupled-cluster singles and doubles (CC2) computations (aug-cc-pVDZ basis functions) were performed with the TURBOMOLE program [20, 21]. The CASSCF calculations were carried out with the GAUSSIAN 03 software package [22].

**Table 3** Theoretical and experimental vibrational frequencies ($cm^{-1}$) of the planar tautomers of cytosine

| A | | | | | B | | | C | | |
|---|---|---|---|---|---|---|---|---|---|---|
| Theor. | Rel. int. | Exp. | Scaled theor.* | Assign. | Scaled theor. | Rel. int. | Assign. | Scaled theor. | Rel. int. | Assign. |
| 1079 | 0.04 | - | 1154 | ν(C–N)+ρ($NH_2$) | 1156 | 0.10 | ρ(H) | 1159 | 0.00 | ρ(H) |
| 1113 | 0.00 | - | 1180 | ρ(H) | 1179 | 0.04 | ρ(H) | 1203 | 0.13 | ρ(H) |
| 1206 | 0.06 | 1235 | 1252 | ρ(H) | 1288 | 0.07 | ρ(H)+ν(C–N) | 1252 | 0.11 | ρ(H) |
| 1263 | 0.03 | 1277 | 1296 | ν(C–N) | 1324 | 0.00 | ν(C–N)+ν(C–C) | 1330 | 0.02 | ρ(H)+ν(C–N) |
| 1349 | 0.07 | 1363 | 1362 | ρ(H)+ν(C-–$N_8$) | 1354 | 0.33 | ν(C–C)+ν(C–N) | 1389 | 0.00 | ρ(H) |
| 1434 | 0.04 | 1463 | 1427 | ν(C–C)+ν(C–N) | 1399 | 0.20 | ν(C–O)+ν(C–N)+ ν(C–$N_8$) | 1400 | 0.06 | ρ(H)+ν(C–N) |
| 1496 | 0.25 | 1504 | 1475 | ν(C–$N_8$) + δ($NH_2$) | 1441 | 0.56 | ν(C–O) | 1427 | 0.05 | ν(C–C)+ν(C-–N) |
| 1567 | 0.12 | 1536 | 1530 | ν(C–C)+ν(C–N) | 1488 | 0.08 | ν(C–N)+ν(C–$N_8$) | 1477 | 0.09 | ν(C–C)+ν(C-–N) |
| 1628 | 0.18 | - | 1576 | ν(C–$N_8$) + δ($NH_2$) | 1556 | 0.38 | ν(C–C)+ν(C–N) | 1566 | 0.03 | ν($N^{im}$=C)+ν(C=C) |
| 1680 | 0.43 | 1610 | 1617 | ν(C=C)+ν(N=C) | 1575 | 0.01 | ν(C=C)+ν(N=C)+δ($NH_2$) | 1630 | 0.28 | ν($N^{im}$=C)+ν(C=C) |
| 1713 | 1.00 | 1660 | 1642 | ν(C=O) | 1605 | 1.00 | ν($N^{im}$=C)+ν(C=C)+ν(N=C) | 1670 | 1.00 | ν(C=O) |
| 3234 | 0.00 | 2678 | 2812 | $\nu_{as}$(C–H) | 2791 | 0.02 | $\nu_{as}$(C–H) | 2816 | 0.00 | $\nu_{as}$(C–H) |
| 3259 | 0.00 | 2782 | 2831 | $\nu_{s}$(C–H) | 2816 | 0.01 | $\nu_{s}$(C–H) | 2834 | 0.00 | $\nu_{s}$(C–H) |
| 3598 | 0.19 | 2997 | 3092 | $\nu_{s}$($NH_2$) | 3099 | 0.19 | $\nu_{s}$($NH_2$) | 3011 | 0.01 | ν($N_8$–H) |
| 3603 | 0.05 | 3163 | 3096 | ν($N_3$–H) | 3187 | 0.17 | ν($O_7$–H) | 3075 | 0.07 | ν($N_1$–H) |
| 3757 | 0.07 | 3378 | 3215 | $\nu_{as}$($NH_2$) | 3218 | 0.11 | $\nu_{as}$($NH_2$) | 3121 | 0.13 | ν($N_3$–H) |

| D | | | E | | | F | | |
|---|---|---|---|---|---|---|---|---|
| Scaled theor. | Rel. int. | Assign. | Scaled theor. | Rel. int. | Assign. | Scaled theoret. | Rel. int. | Assign. |
| 1149 | 0.05 | ρ(H)+ν(C–N) | 1153 | 0.04 | $\nu^{ring}$ | 1143 | 0.01 | ρ(H) |
| 1205 | 0.15 | ρ(H)+ν(C–N) | 1203 | 0.10 | ρ(H) | 1150 | 0.00 | ρ(H) |
| 1251 | 0.29 | ρ(H) | 1251 | 0.55 | ρ(H) | 1206 | 0.01 | ν(C–N)+ρ(H) |
| 1272 | 0.21 | ν(C–O) | 1310 | 0.01 | ν(C–O)+ν(C-N) | 1333 | 0.09 | ν(C–$N_8$) |
| 1346 | 0.03 | ν(C–N)+ν(C–O) | 1352 | 0.00 | ρ(H) | 1372 | 0.09 | ρ(H)+δ(HC=N) |
| 1393 | 0.00 | ν(C–N) | 1361 | 0.09 | ν(C–C)+ν(C–N) | 1398 | 0.02 | ρ(H) |
| 1417 | 0.01 | ν(C–C)+ν(C–O) | 1430 | 0.00 | ν(C–C)+ν(C–N) | 1474 | 0.08 | ν(C–N)+ν(C–O) |
| 1519 | 0.49 | ν(C–N) | 1510 | 0.12 | ν(C=C)+ν(O–C–N) | 1559 | 0.19 | ν(C=N)+ν(C=O) |
| 1536 | 0.43 | ν($N^{im}$=C)+ν(C=C) | 1536 | 0.38 | ν(C=C)+ν(N=C) | 1580 | 0.07 | ν(C=C)+δ($NH_2$) |
| 1593 | 0.05 | ν($N^{im}$=C)+ ν(N=C)+ν(C=C) | 1573 | 1.00 | ν(N=C) | 1610 | 1.00 | ν(C–$N_8$) + δ($NH_2$) + ν(C=C) |

**Table 3** (continued)

| D | | | E | | | F | | |
|---|---|---|---|---|---|---|---|---|
| Scaled theor. | Rel. int. | Assign. | Scaled theor. | Rel. int. | Assign. | Scaled theoret. | Rel. int. | Assign. |
| 1630 | 1.00 | ν(N=C)+ν(C=C) | 1633 | 0.96 | $\nu(N^{im}=C)+\nu(N=C)+\nu(C=C)$ | 1644 | 0.82 | ν(C=O) |
| 2810 | 0.00 | $\nu_{as}$(C–H) | 2798 | 0.02 | $\nu_{as}$(C–H) | 2769 | 0.03 | $\nu_{as}$(C–H) |
| 2830 | 0.01 | $\nu_{s}$(C–H) | 2819 | 0.01 | $\nu_{s}$(C–H) | 2828 | 0.00 | $\nu_{s}$(C–H) |
| 2978 | 0.02 | $\nu(N_8–H)$ | 3014 | 0.03 | $\nu(N_8–H)$ | 3065 | 0.06 | $\nu(N_1–H)$ |
| 3126 | 0.27 | $\nu(N_3–H)$ | 3068 | 0.17 | $\nu(N_1–H)$ | 3106 | 0.15 | $\nu_{s}(NH_2)$ |
| 3178 | 0.21 | $\nu(O_7–H)$ | 3187 | 0.29 | $\nu(O_7–H)$ | 3216 | 0.07 | $\nu_{as}(NH_2)$ |

*The theoretical frequencies were scaled by the equation $f_{exp} = 0.7694 f_{theor} + 323.91$ ($R^2 = 0.9918$), which is the correlation between the theoretical and experimental frequencies of tautomer A of cytosine

## Results and discussion

### Ground-state equilibrium geometries

The ground-state equilibrium geometries of the cytosine and isocytosine tautomers are depicted in Fig. 3 (the atom labeling shown in the figure is used in the discussion below). We obtained planar geometries for all structures. Tautomer A of cytosine shows typical aromatic properties with respect to the ring and the functional groups $–NH_2$ and C=O.

Structure B is amino-hydroxy tautomer of cytosine that also exhibits aromatic properties. Cytosine can form three imino tautomers, designated C, D, and E. The distance C=N in the imino group is rather short: 1.305–1.308 Å, which indicates significant conjugation between this group and the pyrimidine ring. Tautomer F has the same functional groups as tautomer A, but the hydrogen atom $H_{11}$ is bound to the $N_1$ atom of the ring.

Isocytosine has two oxo tautomers: iA and iE. As mentioned above, these two tautomers exist in equal amounts in the solid state [12, 13]. With respect to the oxo-hydroxy tautomerism, only iA is of any real significance. The probability of the proton transfer $N_3…H_{11}…O_8$ (e.g., iE → iB) should be low, as it is associated with substantial redistribution of the π-electron density of the ring. On the other hand, tautomer iE is not available in acetonitrile solution [3].

### Vertical excitation energies

We calculated the vertical excitation energies of the tautomers of cytosine and isocytosine. They are listed in Table 2. The experimental UV spectrum of the unirradiated cytosine solution shows one intense UV-absorption maximum at 203 nm and less intensive maxima at 236 and 271 nm. In agreement with experimental observations, the CC2 vertical excitation energies of tautomer A predicted one intense absorption at 201 nm ($f$=0.316) and two less intense ones at 236 ($f$=0.047) and 271 nm ($f$=0.139). These were all assigned to $\pi \rightarrow \pi^*$ transitions.

Comparing the experimental and calculated vertical excitation energies, we can see that tautomers B and C of cytosine are not available in acetonitrile: there are no experimental bands at about 250 nm. The experimental spectrum does not provide information about tautomer D, since the calculated vertical excitation energies should be included in the experimental UV-absorption bands, as in the case of tautomer A. On the other hand, tautomers E and F are not available in the acetonitrile solution of cytosine, since their vertical excitation energies differ considerably from the experimental UV-absorption maxima. These findings are in full agreement with the experiment of Morita [3].

The slight reduction in the experimental UV-absorption maxima of cytosine during the course of irradiation with

**Table 4** Theoretical and experimental vibrational frequencies ($cm^{-1}$) of the planar tautomers of isocytosine

| iA | | | | | iB | | | | iC | | |
|---|---|---|---|---|---|---|---|---|---|---|---|
| Theor. | Rel. int. | Exp. | Scaled theor.* | Assign. | Scaled theor. | Rel. int. | Exp. | Assign. | Scaled theor. | Rel. int. | Assign. |
| 1042 | 0.00 | - | 1131 | ν(C–N) + ρ(H) | 1145 | 0.01 | 981 | ρ(H) + $\nu^{ring}$ | 1157 | 0.05 | ρ(H) + ν(C–N) |
| 1110 | 0.01 | - | 1184 | ρH | 1190 | 0.02 | 1081 | ρ(H) | 1192 | 0.12 | ρ(H) |
| 1223 | 0.01 | 1232 | 1271 | ν(C–N) + ν(C–C) | 1270 | 0.60 | 1273 | ν(C–O) + ρ(H) + ν(C–N) | 1268 | 0.06 | ρ(H) |
| 1315 | 0.00 | - | 1342 | ν(C–$N_7$) + ρ(H) | 1340 | 0.01 | 1301 | ν(C–N) + ρ(H) | 1306 | 0.04 | ρ(H) + ν(C–N) |
| 1322 | 0.18 | 1409 | 1348 | ν(C–N) + ρ(H) | 1362 | 0.02 | - | ν(C–N) + ν(C–C) | 1395 | 0.00 | ρ(H) |
| 1423 | 0.02 | 1445 | 1426 | ν(C–C) + ρ(H) | 1387 | 0.03 | 1383 | ν(C–O) + $\nu^{ring}$ | 1410 | 0.01 | ρ(H) |
| 1506 | 0.03 | 1474 | 1490 | ν(C–N) | 1465 | 0.37 | - | $\nu^{ring}$ | 1441 | 0.16 | ν(C–$N_7$) |
| 1586 | 0.35 | 1519 | 1552 | ν(C–N) + ν(C–C) | 1474 | 0.36 | 1472 | ν(C–$N_7$) | 1474 | 0.09 | ν(C–N) |
| 1596 | 0.01 | 1565 | 1560 | ν(C=C) + ν(C=N) | 1575 | 0.41 | | ν(C=C) + ν(C=N) | 1598 | 0.01 | ν(C=C) + ν(C=O) |
| 1658 | 1.00 | 1607 | 1608 | ν(C–$N_7$) + δ($NH_2$) + ν(C=N) | 1586 | 0.56 | 1604 | ν(C–C) + ν(C–$N_7$) | 1644 | 0.27 | ν(C=$N_7$) + ν(C=C) + ν(C=O) |
| 1725 | 0.80 | 1678 | 1660 | ν(C=O) + ν(C=C) | 1609 | 1.00 | 1669 | ν(C=N) + ν(C=C) | 1657 | 1.00 | ν(C=$N_7$) + ν(C=C) + ν(C=O) |
| 3207 | 0.02 | 2739 | 2807 | $\nu_{as}$(C–H) | 2805 | 0.03 | 2928 | $\nu_{as}$(C–H) | 2831 | 0.00 | $\nu_{as}$(C–H) |
| 3259 | 0.00 | 2830 | 2848 | $\nu_s$(C–H) | 2852 | 0.00 | 2959 | $\nu_s$(C–H) | 2863 | 0.00 | $\nu_s$(C–H) |
| 3557 | 0.06 | 3141 | 3078 | ν($N_1$–H) | 3126 | 0.24 | 3146 | $\nu_s$($NH_2$) | 3040 | 0.02 | ν($N_7$–H) |
| 3616 | 0.17 | | 3124 | $\nu_s$($NH_2$) | 3190 | 0.18 | ~3290 | ν($O_8$–H) | 3091 | 0.07 | ν($N_1$–H) |
| 3768 | 0.10 | ~3250 | 3242 | $\nu_{as}$($NH_2$) | 3249 | 0.15 | ~3290 | $\nu_{as}$($NH_2$) | 3140 | 0.09 | ν($N_3$–H) |

| iD | | | iE | | | |
|---|---|---|---|---|---|---|
| Scaled theor. | Rel. int. | Assign. | Scaled theor. | Rel. int. | Assign. | Exp. |
| 1163 | 0.05 | ρ(H) + ν(C–N) | 1149 | 0.02 | ν(C–C) + ν(C–N) + ρ(H) | - |
| 1204 | 0.07 | ρ(H) + ν(C–N) | 1190 | 0.01 | ρ(H) | - |
| 1256 | 0.29 | ρ(H) | 1258 | 0.03 | ν(C–N) + ρ(H) | 1232 |
| 1288 | 0.14 | ν(C–O) + ρ(H) | 1319 | 0.10 | ν(C–N) + ν(C–$N_7$) | - |
| 1343 | 0.01 | ν(C–N) + ρ(H) | 1382 | 0.25 | ν(C–$N_7$) + ν(C–N) | 1394 |
| 1381 | 0.00 | $\nu^{ring}$ | 1423 | 0.00 | ν(C–C) + ν(C–N) | - |
| 1448 | 0.08 | ν(C–C) + ν(C–N) | 1500 | 0.42 | $\nu^{ring}$ | 1519 |
| 1479 | 0.17 | ν(C–O) + ν(C–N) | 1559 | 0.58 | $\nu^{ring}$ | 1565 |

**Table 4** (continued)

| iD | | | iE | | | |
|---|---|---|---|---|---|---|
| Scaled theor. | Rel. int. | Assign. | Scaled theor. | Rel. int. | Assign. | Exp. |
| 1564 | 0.07 | $\nu$(N=C) + $\nu$(C=C) + $\nu$($N^{in}$=C) | 1578 | 0.52 | $\nu$(C=C) + $\nu$(C=O) | - |
| 1606 | 0.17 | $\nu$($N^{in}$=C) + $\nu$(N=C) + $\nu$(C=C) | 1623 | 0.66 | $\nu$(C=O) + $\nu$(C=C) | 1607 |
| 1639 | 1.00 | $\nu$($N^{in}$=C) + $\nu$(N=C) + $\nu$(C=C) | 1626 | 1.00 | $\nu$(N=C) + $\nu$(C=C) + $\nu$(C=O) | 1678 |
| 2837 | 0.00 | $\nu_{as}$(C–H) | 2832 | 0.00 | $\nu_{as}$(C–H) | 2739 |
| 2868 | 0.00 | $\nu_{s}$(C–H) | 2849 | 0.00 | $\nu_{s}$(C–H) | 2830 |
| 3039 | 0.03 | $\nu$($N_7$–H) | 3123 | 0.21 | $\nu_{s}$($NH_2$) | - |
| 3112 | 0.12 | $\nu$($N_3$–H) | 3137 | 0.18 | $\nu$($N_3$–H) | 3141 |
| 3176 | 0.10 | $\nu$($O_8$–H) | 3241 | 0.15 | $\nu_{as}$($NH_2$) | ~3250 |

The theoretical frequencies were scaled by the equation $f_{exp} = 0.7744 f_{theor} + 323.93$ ($R^2 = 0.9974$), which is the correlation between the theoretical and experimental frequencies for tautomer iA of isocytosine

UV light might be due to the photodecomposition of the compound. This photoreaction is not of interest in the current study. In general, cytosine is quite stable upon UV irradiation.

The experimental UV-absorption maxima of the acetonitrile solution of unirradiated isocytosine are at 287 nm and 222 nm. We assigned these bands to the $\pi \rightarrow \pi^*$ and $n_O \rightarrow \sigma^*$ electron transitions of tautomer iA of isocytosine. The calculated vertical excitation energies of tautomers iA, iB, and iE show that the signals of the bright states of these tautomers should overlap with the broad experimental absorption bands. In other words, these tautomers cannot be identified from the UV spectrum of unirradiated isocytosine. Most probably, tautomers iC and iD are not available in the acetonitrile solution of unirradiated isocytosine.

The irradiated solution of isocytosine shows reductions in the intensities of the UV-absorption maxima. Perhaps this is due to a first-order reaction in which isocytosine participates (Fig. 1). There is an accompanying reaction that is probably the photodecomposition of isocytosine [3]. Such decay reactions are not of interest in the current study. We are looking for phototautomeric reactions through excited states. As Vranken mentioned [14], the irradiation of isocytosine leads to the formation of the amino-hydroxy form, which is in accord with the IR spectra of irradiated and unirradiated isocytosine (see below). Unfortunately, the UV-absorption spectrum of irradiated cytosine solution is not informative enough to allow the photoproduct(s) to be identified.

## Vibration spectra

The characteristic theoretical and experimental (KBr disc) vibrational frequencies of cytosine and isocytosine above 1000 $cm^{-1}$ are compared in Tables 3 and 4. Selected regions of the vibrational spectra of unirradiated and irradiated isocytosine are given in Fig. 4.

Upon comparing the experimental and theoretical vibrational frequencies of cytosine (Table 3), we identified tautomer A as a stable form in the solid state, in accord with other experimental investigations [3, 5]. The data in Table 3 were used to find a correlation between the theoretical and experimental frequencies. We estimated the following correlation equation: $f_{exp} = 0.7694 f_{theor} + 323.91$, with a correlation coefficient of 0.9918. This equation was used to scale the calculated frequencies of the remaining tautomers of cytosine. The experimental spectra of irradiated and unirradiated cytosine are identical, which means that this compound is relatively photostable.

In accord with crystallographic investigations [12, 13], the experimental and theoretical vibrational frequencies (Table 4) of unirradiated isocytosine imply the presence of two stable oxo tautomers of isocytosine (iA and iE). Most of the bands of

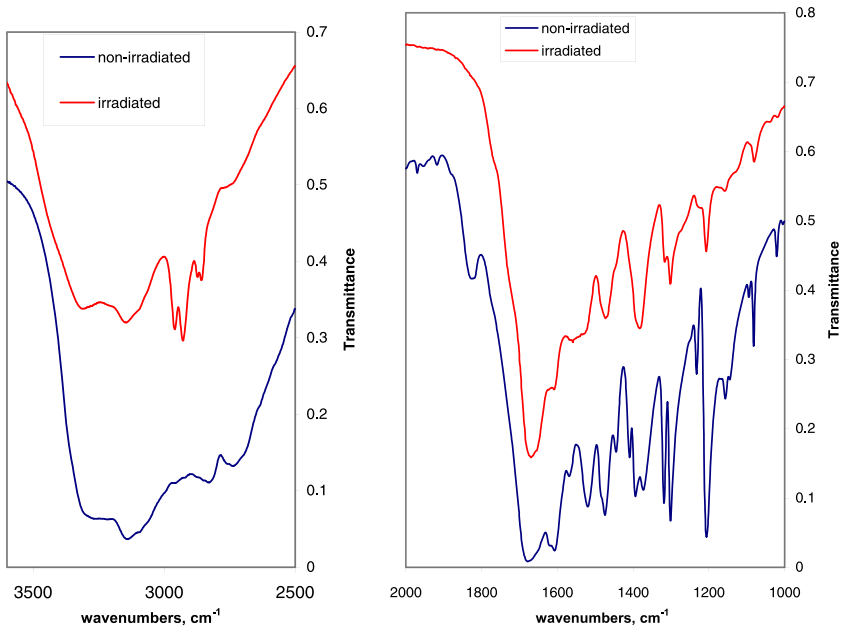


**Fig. 4** IR spectra of unirradiated and irradiated isocytosine recorded in KBr discs

the two tautomers suffer from extensive overlapping, so explicit recognition of tautomers iA and iE is not possible.

We found a correlation between the theoretical and experimental vibrational frequencies of tautomer iA: $f_{exp} = 0.7744 f_{theor} + 323.93$ ($R^2 = 0.9974$). The calculated vibrational frequencies of the remaining tautomers of isocytosine were scaled by this equation.

Figure 4 shows the differences between the vibrational spectra of unirradiated and irradiated isocytosine. In both spectra, the bands above 3000 $cm^{-1}$ are rather diffusive and suffer from heavy overlapping. For unirradiated isocytosine, the bands of the characteristic $NH_2$ stretching vibrations are almost fully obscured due to overlapping. There are intense bands for the C=O, C=C, and C=N stretching vibrations at 1678 $cm^{-1}$ and 1607 $cm^{-1}$. As proposed by Vranken [14], the vibrational spectrum of irradiated isocytosine indicates the presence of amino-hydroxy tautomer iB. The OH band of tautomer iB is

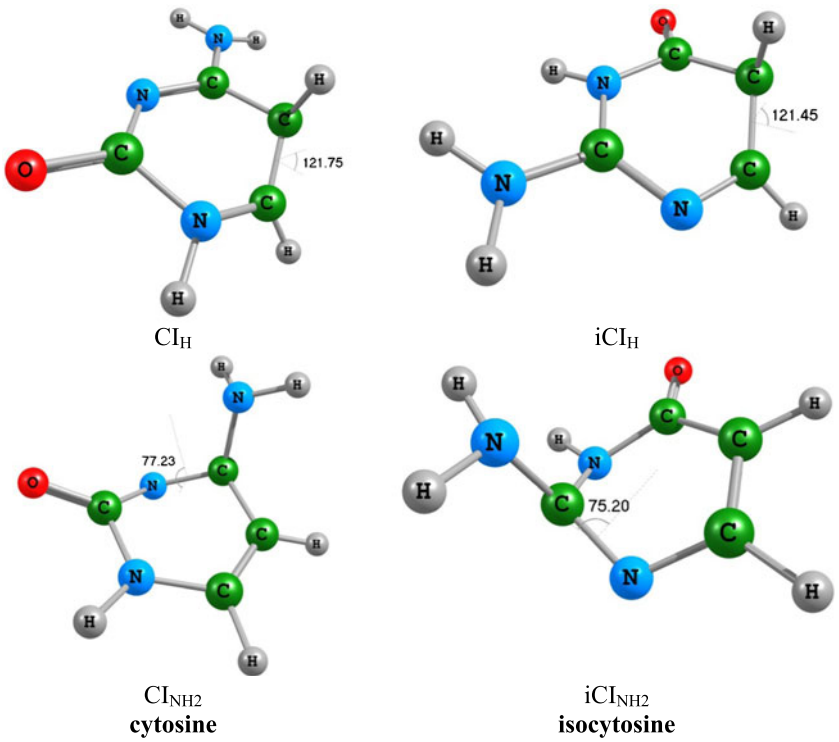


**Fig. 5** CASSCF(6,6)-optimized structures of the conical intersections of cytosine and isocytosine

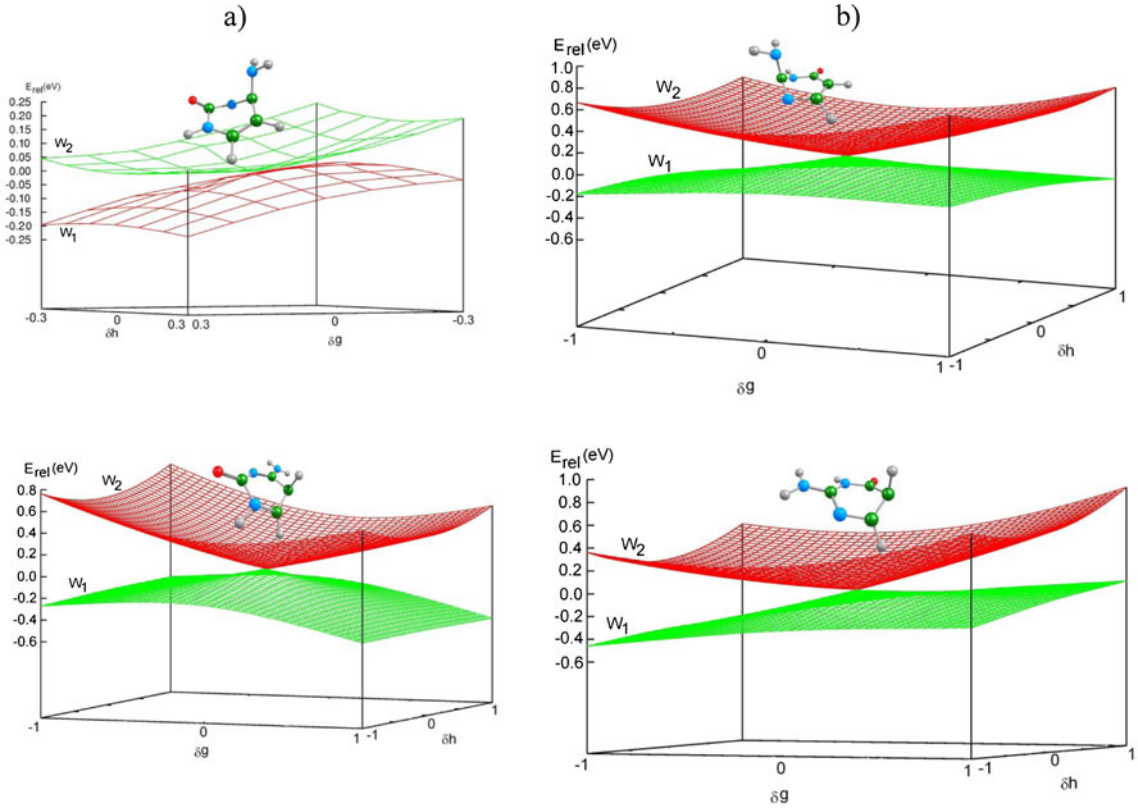


**Fig. 6a–b** Adiabatic PESs near (*narrow grid*) the conical intersections $CI_{NH2}$ and $CI_H$ of **a** cytosine and **b** isocytosine ($iCI_{NH2}$ and $iCI_H$). The surfaces were constructed using the energies of the two states obtained from the ab initio calculations (7×7=49 points—geometries). The ab initio energies were calculated at the CASSCF(6,6)/6-31 G* level

overlapped by the $NH_2$ bands of tautomers iA and iE (Fig. 4). However, the asymmetric and symmetric C–H vibrations of the irradiated sample show clear bands at 2958 $cm^{-1}$ and 2930 $cm^{-1}$. These bands are slightly redshifted compared to the unirradiated isocytosine (tautomers iA and iE). The same shift was predicted for the theoretical vibrational frequencies. The C–O stretching vibration of tautomer iB was noted at 1273 $cm^{-1}$ and calculated (scaled) to occur at 1270 $cm^{-1}$. The bands at 1519 $cm^{-1}$ and 1474 $cm^{-1}$, which are assigned to the ν(C–N) and ν(C–C) vibrations in tautomer iA, disappear after irradiating isocytosine (in tautomer iB). The same behavior was exhibited by the band at 1232 $cm^{-1}$ of tautomer iA.

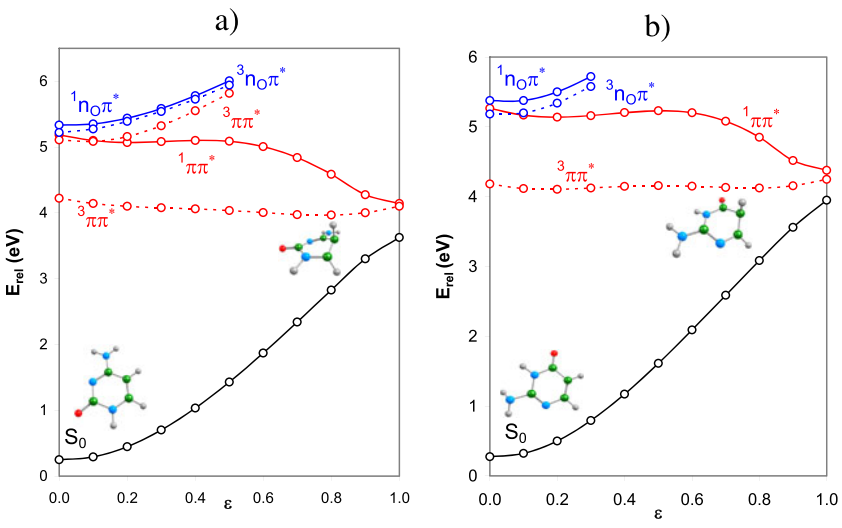


**Fig. 7a–b** Excited-state reaction paths (linearly interpolated) for the transformations **a** A → $CI_H$ and **b** iA → $iCI_H$. The energies of the CC2-ground-state equilibrium geometries of tautomers A and iB were used as a reference values (−393.934561 a.u. and −393.936624 a.u.) to find the relative energies. The reaction paths of the singlet excited states and $S_0$ are indicated by *solid curves*, while the reaction paths of the triplet excited states are illustrated by *dashed curves*

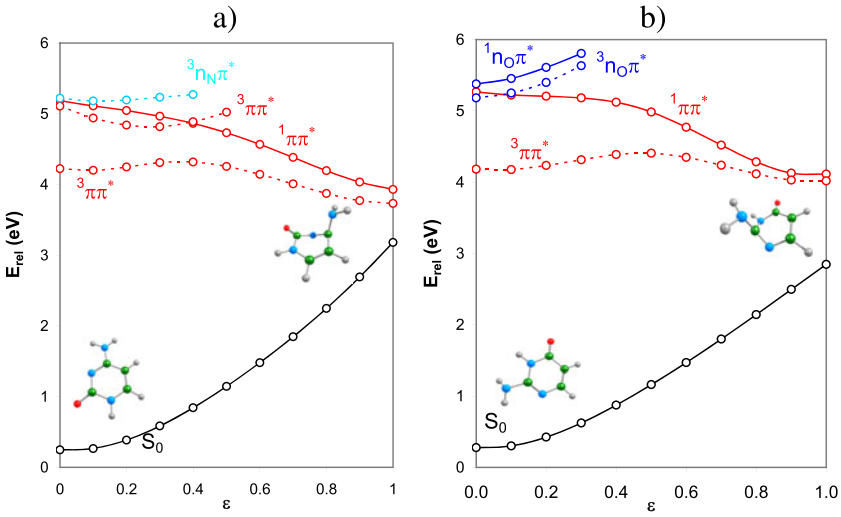


**Fig. 8a–b** Excited-state reaction paths (linearly interpolated) for the transformations **a** A → $CI_{NH2}$ and **b** iA → $iCI_{NH2}$. The energies of the CC2-ground-state equilibrium geometries of tautomers A and iB were used as reference values (−393.934561 a.u. and −393.936624 a.u.) to find the relative energies. The reaction paths of the singlet excited states and $S_0$ are denoted by *solid curves*, while the reaction paths of the triplet excited states are denoted by *dashed curves*

## Excited-state reaction paths

In order to explain the different photophysical properties of cytosine and isocytosine with respect to the UV irradiation, we investigated the excited-state reaction paths of two major mechanisms: deformations of the aromatic rings and N–H bond dissociations. It is well known that the radiationless deactivation of the excited states of pyrimidine bases occurs via internal conversion and conical intersections $S_0/S_1$ [23–26]. The ring deformations are usually associated with C=C twisting [26, 27].

This study is limited to tautomers A and iA, since they are the most stable amino-oxo tautomers available in the solid state and in solution. Four conical intersections $S_0/S_1$ were optimized (via CASSCF/6-31 G*) for the ring deformations. Their geometries are illustrated in Fig. 5.

The conical intersections $CI_H$ and $iCI_H$ are obtained via C=C twisting, whereas the conical intersections $CI_{NH2}$ and $iCI_{NH2}$ are accessible by deformations of the rings at the $NH_2$ groups. The structures of both conical intersections of cytosine are well known [24–26, 28], but those of isocytosine ($iCI_H$ and $iCI_{NH2}$) are not—this is the first time that they have been presented.

To prove that the found structures are real conical intersections $S_0/S_1$, we constructed the adiabatic surfaces $W_1$ and $W_2$ on a narrow grid around the conical intersections. These are depicted in Fig. 6. The adiabatic PESs were constructed using the ab initio energies of the two electronic states for 49 structures (points) around each conical intersection. For the conical intersections $iCI_H$, $CI_{NH2}$, and $iCI_{NH2}$, we interpolated between the calculated ab inito energies to construct the adiabatic surfaces (thicker grids). The adiabatic surfaces in Fig. 6 show the deactivation paths for the excited state via conical intersections. Depending on the slope of the potential energy surface from the conical intersection, the photoreactions proceed in a particular direction, leading to related photoproduct(s).

Figure 7 shows the linearly interpolated excited-state reaction paths for C=C twisting in cytosine and isocytosine.

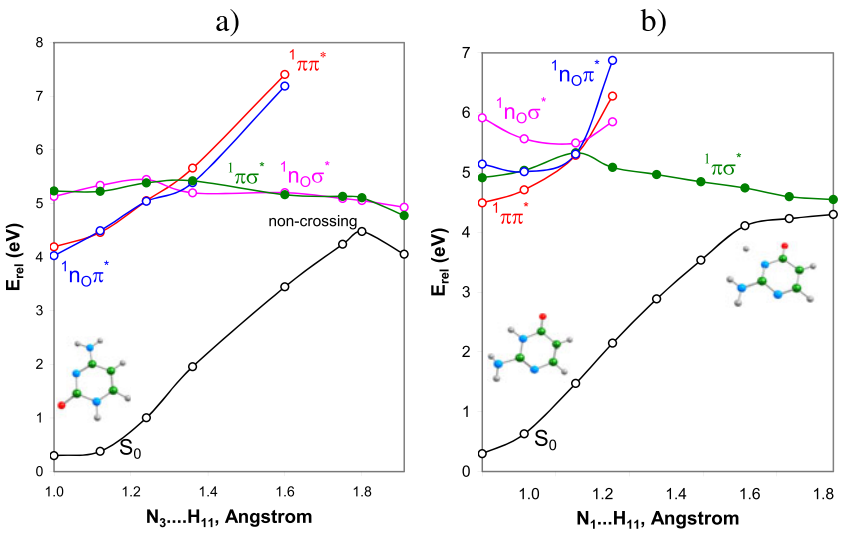


**Fig. 9a–b** Coordinate-driven excited-state reaction paths (relaxed scans) for the **a** $N_3$–H dissociation of tautomer A and **b** $N_1$–H dissociation of tautomer iA. Optimizations of the low-lying $^1\pi\sigma^*$ excited-state reaction paths were performed (*full circles*). The energies of the CC2-ground-state equilibrium geometries of tautomers A and iB were used as reference values (−393.934561 a.u. and −393.936624 a.u.) to find the relative energies

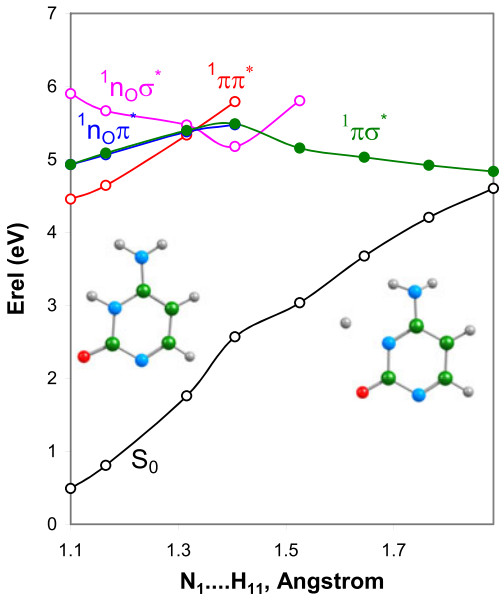


**Fig. 10** Coordinate-driven excited-state reaction paths (relaxed scans) for the $N_1$–H dissociation of tautomer F. Optimization of the low-lying $^1\pi\sigma^*$ excited-state reaction path was performed (*full circles*). The energy of the CC2-ground-state equilibrium geometry of tautomer A was used as a reference value (−393.934561 a.u.) to find the relative energies

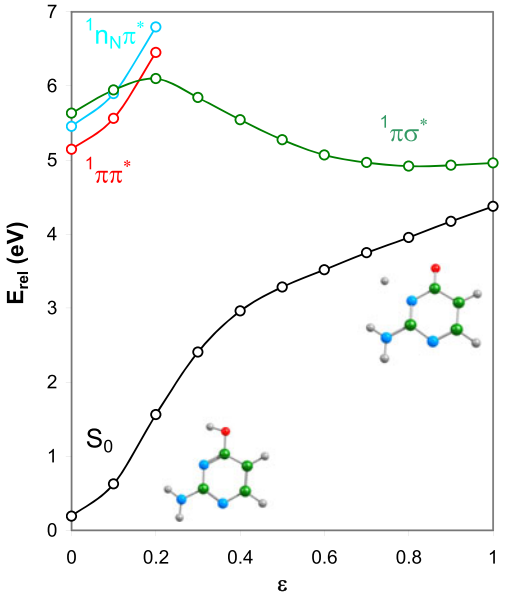


**Fig. 12** Excited-state reaction paths (linearly interpolated) for the transformation iB → $iCI_{N...H}$. The energy of the CC2-ground-state equilibrium geometry of tautomer iB was used as a reference value (−393.936624 a.u.) to find the relative energies

Linear interpolation was performed between the CASSCF-optimized structures of the ground-state minimum and the conical intersection. The $^1\pi\pi^*$ excited-state reaction paths of cytosine and isocytosine exhibit almost identical features with respect to this mechanism (Fig. 7): relaxation of the $^1\pi\pi^*$ excited states via conical intersections $S_0/S_1$. It should be noted that these conical intersections are crossing points between two singlet excited states ($S_0$ and $^1\pi\pi^*$) and one $^3\pi\pi^*$ triplet excited state. In other words, the conical intersections $S_0/S_1$ can mediate the intercombination processes: populating the low-lying $^3\pi\pi^*$ triplet states from the singlet $^1\pi\pi^*$ excited states.

The mechanisms of the ring deformations at the $NH_2$ groups of cytosine and isocytosine (Fig. 8) lead to the same conclusions as those obtained for the C=C twisting. It can be concluded that the two compounds should be photostable with respect to these deformation mechanism. Relaxations of the $^1\pi\pi^*$ excited states by ring deformations should be expected on picosecond or/and femtosecond timescales.

In order to determine the possibility of phototautomerization, we performed relaxed scans of $^1\pi\sigma^*$ excited states for N–H dissociations ($C_S$ symmetry restrictions). The $^1\pi\sigma^*$ excited states were optimized (CC2/aug-cc-pVDZ) along the N–H reaction coordinates. The results are illustrated in Fig. 9. As seen, the $^1\pi\sigma^*$ excited-state reaction path of cytosine (Fig. 9a) does not lead to a crossing with the ground state $S_0$. At some points along the reaction coordinate, the $^1\pi\sigma^*$ excited state of cytosine is quasidegenerate with the bright $^1n_O\sigma^*$ excited state. We did not find any conical intersection $S_0/S_1$ for this mechanism.

Sharonov et al. [29] have measured a ps-fluorescent transition of cytosine with a large Stokes shift of about 0.86 eV. Our study shows that the fluorescent transition $^1n_O\sigma^* \rightarrow {}^1\pi\pi^*$ leads to a Stokes shift of about 0.94 eV with

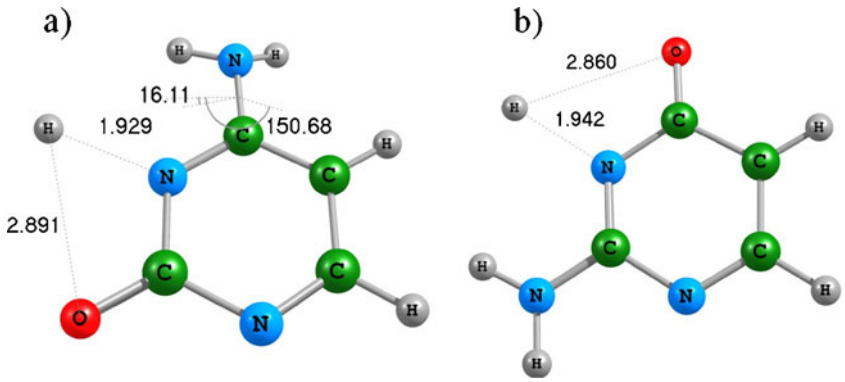


**Fig. 11a–b** CASSCF-optimized conical intersections $S_0/S_1$ of the N–H dissociation mechanisms of **a** cytosine ($CI_{N...H}$) and **b** isocytosine ($iCI_{N...H}$)

respect to the vertical excitation energy of the $^1n_O\sigma^*$ excited state. In other words, the N–H dissociation of cytosine cannot occur by the $^1\pi\sigma^*$ excited-state reaction path.

The $N_1$–H dissociation mechanism of the amino-oxo N(1)H tautomer F of cytosine (Fig. 10) does not lead to an ultrafast relaxation of the $^1\pi\sigma^*$ excited state through the conical intersection $S_0/S_1$, since the excited system is trapped in the minimum of the $^1n_O\sigma^*$ excited state. In other words, only fluorescent processes leading to the ground state of tautomer F should be expected. The conical intersection $S_0/S_1$ that we found (Fig. 11a) shows a large deviation of the hydrogen atoms of the amino group from the molecular plane.

The relaxed scan of isocytosine is illustrated in Fig. 9b. In this case, we found a conical intersection $S_0/S_1$ which mediates the radiationless relaxation of the $^1\pi\sigma^*$ excited state. The conical intersection is planar (Fig. 11b) and it is accessible through the $^1\pi\sigma^*$ excited state of the N–H dissociation mechanism. The excited-state reaction paths in Fig. 9 show that the $^1\pi\sigma^*$ excited state can be populated in two ways: via the bright $^1\pi\pi^*$ excited state and a conical intersection $^1\pi\pi^*/\,^1\pi\sigma^*$ (this process passes through an energy barrier of 0.797 eV); from the minimum of the bright $^1n_O\sigma^*$ excited state and a fluorescent transition (0.165 eV) to the $^1\pi\sigma^*$ excited state.

We expected that the aforementioned mechanism could lead to the association of the dissociated proton with the oxygen atom. In order to check this association process, we performed linear interpolation between the CASSCF-optimized structure of tautomer iB and the conical intersection $iCI_{N\ldots H}$. The mechanism is illustrated in Fig. 12. As seen, the relaxation of the system from the conical intersection $iCI_{N\ldots H}$ can proceed, in a barrierless manner, to the stabilization of the ground state of tautomer iB. The reverse radiationless process is hindered by the energy barrier (about 0.5 eV) of the $^1\pi\sigma^*$ excited-state reaction path. This fact shows that the UV-irradiation process of isocytosine would lead to the accumulation of the amino-hydroxy tautomer as the main photoproduct.

## Conclusions

We performed an experimental and theoretical study of the photostabilities of two position isomers: cytosine and isocytosine. Experimental analysis of the stability of the compounds upon UV irradiation showed that cytosine is relatively photostable, while isocytosine isomerizes to the amino-hydroxy tautomer.

The theoretical investigation (relaxed scan, linear interpolation in internal coordinates) showed that the $^1\pi\pi^*$ excited states of cytosine and isocytosine, in a barrierless manner, relax (internal conversion) to the ground states of the amino-oxo forms of the compounds. These processes occur by ring deformations and conical intersections $S_0/S_1$. In other words, the two compounds should be photostable with respect to these mechanisms. However, for isocytosine, we found a nonradiative $^1\pi\sigma^*$ deactivation channel that is responsible for the phototautomerization of isocytosine to the amino-hydroxy form. This channel follows the so-called PIDA mechanism, which occurs through the repulsive $^1\pi\sigma^*$ excited state [19, 25, 30].

**Acknowledgments** One of us (VBD) thanks the National Science Fund of Bulgaria, project RNF01/0110, for their financial support of the calculations (Linux cluster MADARA). We thank Assoc. Prof. Dr Plamen Penchev and Mrs. Neda Danova (Dept. Analytical Chemistry, University of Plovdiv) for the experimental registration of the UV and IR spectra.

## References

1. Fülscher MP, Roos BO (1995) J Am Chem Soc 117:2089–2095
2. Ismail N, Blancafort L, Olivucci M, Kohler B, Robb MA (2002) J Am Chem Soc 124:6818–6819
3. Morita H, Nagakura S (1968) Theor Chim Acta (Berl) 11:279–295
4. Brown DJ, Lyall JM (1962) Australian J Chem 15:851–857
5. Jeffrey GA, Kinoshita Y (1963) Acta Cryst 16:20–28
6. Szczesniak M, Szczesniak K, Kwiatowski JS, KuBulat K, Person WB (1988) J Am Chem Soc 110:8319–8330
7. Nir E, Műller M, Grace LI, de Vries MS (2002) Chem Phys Lett 355:59–64
8. Brown RD, Godfrey PD, McNaughton D, Pierlot AP (1989) J Am Chem Soc 111:2308–2310
9. Tomić K, Tatchen J, Marian CM (2005) J Phys Chem A 109:8410–8418
10. Kosma K, Schröter Ch, Samoylova E, Hertel IV, Schultz T (2009) J Am Chem Soc 131:16939–16943
11. Canuel C, Mons M, Piuzzi F, Tardivel B, Dimicoli I, Elhanine M (2005) J Chem Phys 122(6):074316
12. Barker D, Marsh RE (1964) Acta Cryst 17:1581–1587
13. Tulub AA, Semenov SG, Stetsenko AI, Yudovich EE (1988) Teoreticheskaya i Eksperimental'naya Khimiya 24:29–36
14. Vranken H, Smets J, Maest G (1994) Spectrochim Acta A 50:875–889
15. Shukla MK, Leszczynski J (2000) Int J Quant Chem 77:240–254
16. Shukla MK, Mishra PC (1999) Chem Phys 240:319–329
17. Barbatti M, Aquino AJA, Szymczak JJ, Nachtigallova D, Lischka H (2011) Phys Chem Chem Phys 13:6145–6155
18. Barbatti M, Aquino AJA, Szymczak JJ, Nachtigallova D, Hobza P, Lischka H (2010) Proc Natl Acad Sci USA 107:21453–21458
19. Chmura B, Rode M, Sobolewski A, Lapinski L, Nowak M (2008) J Phys Chem A 112:13655–13661
20. Ahlrichs R, Baer M, Haeser M, Horn H, Koelmel C (1989) Chem Phys Lett 162:165–169
21. Hättig C, Weigend F (2000) J Chem Phys 113:5154–5161
22. Frisch MJ, Trucks GW, Schlegel HB, Scuseria GE, Robb MA, Cheeseman JR, Montgomery JA-Jr, Vreven T, Kudin KN, Burant JC, Millam JM, Iyengar SS, Tomasi J, Barone V, Mennucci B, Cossi M, Scalmani G, Rega N, Petersson GA, Nakatsuji H, Hada M, Ehara M, Toyota K, Fukuda R, Hasegawa J, Ishida M, Nakajima T, Honda Y, Kitao O, Nakai H, Klene M, Li X, Knox JE, Hratchian HP, Cross JB, Bakken V, Adamo C, Jaramillo J, Gomperts R, Stratmann RE, Yazyev O, Austin AJ, Cammi R, Pomelli C, Ochterski JW, Ayala PY, Morokuma K, Voth GA, Salvador P, Dannenberg JJ, Zakrzewski VG, Dapprich S, Daniels AD, Strain MC, Farkas O, Malick DK, Rabuck AD, Raghavachari K, Foresman JB, Ortiz JV,

Cui Q, Baboul AG, Clifford S, Cioslowski J, Stefanov BB, Liu G, Liashenko A, Piskorz P, Komaromi I, Martin RL, Fox DJ, Keith T, Al-Laham MA, Peng CY, Nanayakkara A, Challacombe M, Gill PMW, Johnson B, Chen W, Wong MW, Gonzalez C, Pople JA (2004) Gaussian 03, revision D.01. Gaussian Inc, Wallingford
23. Matsika S (2004) J Phys Chem A 108:7584–7590
24. Matsika S (2005) J Phys Chem A 109:7538–7545
25. Delchev VB, Sobolewski AL, Domcke W (2010) Phys Chem Chem Phys 12:5007–5015
26. Merchan M, Gonzalez-Luque R, Climent T, Serrano-Andres L, Rodriguez E, Reguero M, Pelaez D (2006) J Phys Chem B 110:26471–26476
27. Levine BG, Martinez TJ (2007) Annu Rev Phys Chem 58:613–634
28. Kistler KA, Matsika S (2008) J Chem Phys 128(14):215102
29. Sharonov A, Gustavsson T, Carre V, Renault E, Markovitsi D (2003) Chem Phys Lett 380:173–180
30. Sobolewski AL (1993) Chem Phys Lett 211:293–299